Electron Confinement in Channel Spaces for One-Dimensional Electride

ARTICLE *in* JOURNAL OF PHYSICAL CHEMISTRY LETTERS · NOVEMBER 2015

Impact Factor: 7.46 · DOI: 10.1021/acs.jpclett.5b02283

4 AUTHORS, INCLUDING:

Zewen Xiao

University of Toledo

14 PUBLICATIONS **20** CITATIONS

THE JOURNAL OF PHYSICAL CHEMISTRY Letters

Letter

pubs.acs.org/JPCL

Electron Confinement in Channel Spaces for One-Dimensional Electride

Yaoqing Zhang,[†,§,⊥] Zewen Xiao,[†,‡,∥,⊥] Toshio Kamiya,[†,‡] and Hideo Hosono*[,†,‡,§]

[†]Materials Research Center for Element Strategy, Tokyo Institute of Technology, Yokohama 226-8503, Japan

[‡]Materials and Structures Laboratory, Tokyo Institute of Technology, Yokohama 226-8503, Japan

[§]ACCEL Project, Japan Science and Technology Agency (JST), Tokyo 102-8666, Japan

Supporting Information

ABSTRACT: Electrides are characteristic of anionic electrons trapped at the structural voids in the host lattice. Electrides are potentially useful in various technological applications; however, electrides, particularly their inorganic subgroup, have been discovered only in limited material systems, notably zero-dimensional $[Ca_{24}Al_{28}O_{64}]^{4+}:4e^-$ and two-dimensional $[Ca_2N]^+:e^-$ and $[Y_2C]^{1.8+}:1.8e^-$. Here, on the basis of density functional theory calculations, we report the first one-dimensional (1D) electride with a $[La_8Sr_2(SiO_4)_6]^{4+}:4e^-$ configuration, in which the four anionic electrons are confined in the channel spaces of the host material. According to this theoretical prediction, an insulator−semiconductor transition originating from electron confinement in the crystallographic channel sites was demonstrated experimentally, where 10.5% of the channel oxygen was removed by reacting an oxygen stoichiometric $La_8Sr_2(SiO_4)_6O_2$ precursor with Ti metal at a high temperature. This study not only adds an unprecedented role to silicate apatite as a parent phase to a new 1D electride, but also, and more importantly, demonstrates an effective approach for developing new electrides with the assistance of computational design.

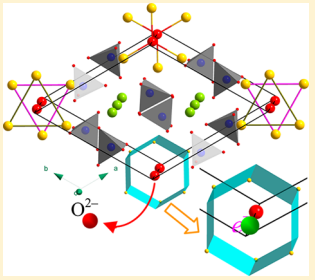

As observed in F-centers[1] in which the created anionic vacancies capture available electrons forming quantum confinement states, one may expect an exotic class of materials, provided similar electron trapping is realized, in compounds with cavity spaces of appropriate topology and size. Indeed, this consideration corresponds to the fundamental principle in designing an electride, which was proposed by Dye[2,3] and is a novel concept material that is defined as a stoichiometric ionic compound in which an electron behaves as an anion.

The earliest synthesized electrides utilized organic molecules that complexed the alkali cations while the released electrons, as a result of the ionization of alkali metals, occupy cavity sites separated from the cations.[4−13] These crystalline organic electrides provide examples demonstrating the wide range of electronic and magnetic properties electride materials can deliver, such as low work function,[14] catalytic activity,[14] and antiferromagnetism.[15] More importantly, these practically useful properties proved to depend on the geometry of the trapping spaces as well as their connectivity.[14,15] Such dependence holds the key to the theoretically directed synthesis of new electrides. On the other hand, the trapped electrons in all known organic electrides tend to destabilize above about −40 °C. There were very few thermal stable electrides at ambient temperatures until the successful synthesis of $[Ca_{24}Al_{28}O_{64}]^{4+}:4e^-$, the first inorganic electride which resists reaction with either air or moisture.[16−18] This stable electride builds upon the well-defined cage space of diameter ∼0.4 nm that is otherwise filled by active oxygen species in the precursor compound, $12CaO{\cdot}7Al_2O_3$ (C12A7).[19−21] Through a simple high-temperature reaction with a reducing agent such as Ca or Ti, the cage-trapped O^{2-} anions can be replaced with stoichiometric electrons.[22] Apparently, the electride materials break the standard valency rules of constituent ions: there is an electron excess if the charge is counted in light of the formal valence of the ions constituting a crystal. It is the strong donating power of these excess electrons in C12A7:$2e^-$ that enables the splitting of carbon dioxide at room temperature and synthesis of ammonia from atmospheric nitrogen under mild conditions.[23−25]

Clearly, the C12A7:e^- electride can be categorized into the zero-dimensional (0D) type if merely considering the geometry of electron-trapping cavity sites, although its Fermi surface remains three-dimensional (3D). Recently, the first two-dimensional (2D) electride, dicalcium nitride, was also realized following an earlier theoretical prediction.[26,27] This discovery represents an essential step toward the higher degree of freedom in dimensionality for electride materials. The crystal structure of Ca_2N structure is of a layered anti-$CdCl_2$ type. Because the formal charge of Ca/N is 2+/3−, compensating electrons are injected in the interlayer free space between the adjacent positively charged planes of $[Ca_2N]^+$, whose electrons are not delocalized as free electron gas but confined to the interlayer spaces, resulting in an electride structure represented by $Ca_2N:e^-$. Like a typical 2D electronic system, the Fermi surface of $Ca_2N:e^-$, composed of the anionic electrons, is cylindrical. Unfortunately, these loosely bound excess electrons

Received: October 13, 2015
Accepted: November 30, 2015

DOI: 10.1021/acs.jpclett.5b02283
J. Phys. Chem. Lett. 2015, 6, 4966−4971

render the electride too reactive with oxygen and moisture in the ambient atmosphere. More recently, some plausible candidates have been further proposed from first-principles electronic structure calculations which allow the systematic screening of a huge set of candidate materials in a database by examining a few key attributes of the 2D electride.[26,28] These calculations have proved they are actually a powerful means, leading to experimental verifications, e.g., in Y_2C.[29,30] These achievements prompt us to further extend the dimensionality of electride systems to 1D because 1D electron confinement may help to suppress the thermal instability and air sensitivity of the existing electrides without seriously compromising their reactivity with species of interest.

Here we consider apatite as a host candidate which meets the essential structural attributes required for an electride. Figure 1

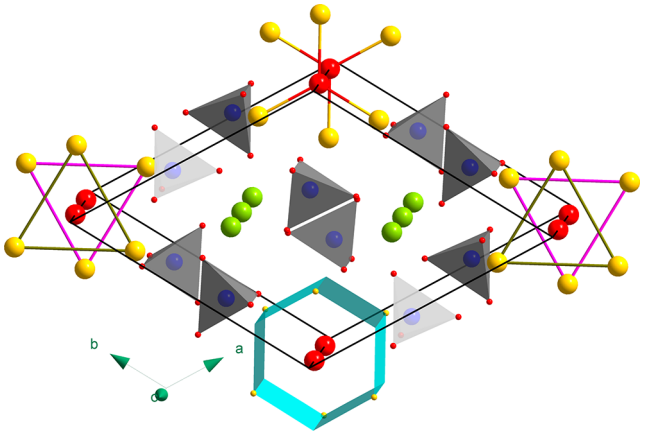

Figure 1. Crystal structure of $La_8Sr_2(SiO_4)_6O_2$. The yellow La(6*h*) cations are arranged in the equilateral triangular geometry and define the characteristic channel spaces. Along the apatite channel (highlighted in cyan) are the red O(2*a*) ions at z = 0.25 and 0.75. The La and Sr atoms sitting at the 4*f* sites are green.

is an illustration of the crystal structure for one silicate variant of apatite, $La_8Sr_2(SiO_4)_6O_2$, which is hexagonal with space group $P6_3/m$. A prominent feature of the apatite structure is the presence of large *c*-axis channels defined by two triangles formed of the 6*h* $[La^{3+}]_3$ at the crystallographic heights z = 1/4 and 3/4, which are rotated by 60° from each other. At the center of the channel structure is the 6-fold screw axis along which the filling anions such as O^{2-} are accommodated at 2*a* sites (0, 0, 1/4). Such an apatite mineral is known for the mobile nature of O(2*a*) at elevated temperatures and the adaptive framework that allows many possibilities in chemistry at the channel and cation sites.[31,32] For instance, the oxygen stoichiometric composition $La_8Sr_2(SiO_4)_6O_2$ is an oxide ion conductor. In response to higher La^{3+}/Sr^{2+} ratios, interstitial oxygen can be registered at the channel to further strengthen the ionic conduction.[33,34] As a result, a simple scenario is that if the mobile 2*a* anions are removed, e.g., by metal reduction, the resulting crystal is likely to form an electride because all cations possess stable valence and the charge balance has to be maintained.

First, density functional theory (DFT) calculations were performed for $La_8Sr_2(SiO_4)_6O_2$ and its oxygen substoichiometric derivatives $La_8Sr_2(SiO_4)_6O_{2-x}$ using the local density approximation (LDA) functional and the projector augmented wave (PAW) method implemented in the VASP 5.3 code.[35] The valence states consist of La 5*s*, 5*p*, 6*s*, 5*d*, 4*f* functions for La; 4*s*, 4*p*, 5*s*, 4*d* functions for Si; 3*s*, 3*p*, 3*d* functions for Si; and O 2*s*, 2*p*, 3*d* functions for O. A Hubbard U correction was applied to the La 4*f* electrons using the Dudarev's + U approach with effective on-site Coulomb interaction U = 11.0 eV and exchange parameter J = 0.36 eV.[36] The plane wave cutoff was set to 500 eV. A 6 × 6 × 8 Γ-centered k-mesh was used to sample the first Brillouin zone. Prior to static electronic calculations, variable-cell structural relaxation was performed to acquire the ground-state structure. In the studied crystals the 6*h* sites are filled exclusively by La whereas the 4*f* sites are equally occupied by Sr and remaining La, yielding three possible partitions of La/Sr atoms into the four 4*f* sites within the unit cell (Figure S1 in Supporting Information). Examinations of all cases showed that the lattice parameters and electronic structures are comfortably independent of the 4*f* La/Sr configuration (see Table S1 and Figure S2). Consequently, discussing one configuration provides understanding of this system.

Figure 2a shows the band structure of $La_8Sr_2(SiO_4)_6O_2$ where a direct band gap of 4.90 eV indicates the intrinsic

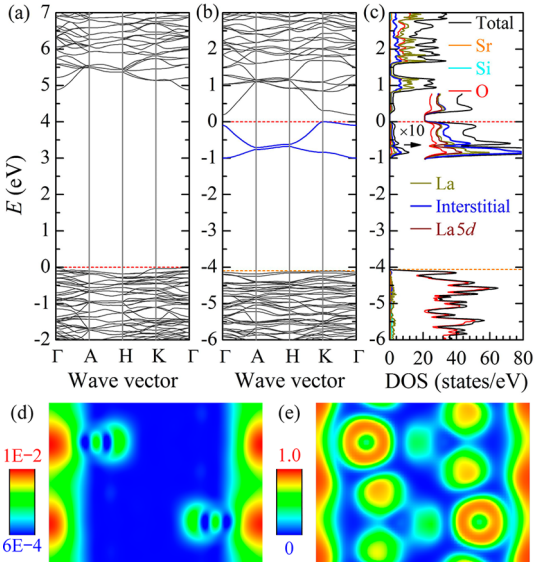

Figure 2. (a) Band structure of $La_8Sr_2(SiO_4)_6O_2$. (b) Band structure and (c) total/projected densities of states (DOSs) of $La_8Sr_2(SiO_4)_6$. For comparison, the energies for $La_8Sr_2(SiO_4)_6O_2$ and $La_8Sr_2(SiO_4)_6$ are aligned by O 2s orbitals. (d) Electron density for the occupied states of the interstitial bands (E = −1.0 to 0 eV) and (e) electron localization function (ELF) map on the $(1\bar{1}00)$ plane parallel to the *c*-axis of $La_8Sr_2(SiO_4)_6$.

insulating nature of the material. The valence band (between −5.70 and 0 eV) consists of O 2*p* orbitals, among which those of O at 2*a* sites contribute to the valence band maximum (VBM) because of their shallow energy levels (Figure S3), while the conduction band minimum (CBM) is dominated by La 5*d* orbitals. Panels b and c of Figure 2 show the band structure and total/projected densities of states (DOSs) of oxygen-deficient $La_8Sr_2(SiO_4)_6$, respectively. In contrast, when two O(2*a*) atoms are completely extracted from this oxygen stoichiometric phase, a slightly lower VBM is observed in the resulting $[La_8Sr_2(SiO_4)_6]^{4+}$ framework (FVBM) as the corresponding six shallow O 2*p* bands are simultaneously removed. On the other hand, the released four electrons in compensation for the oxygen deficiency generate two new

DOI: 10.1021/acs.jpclett.5b02283
J. Phys. Chem. Lett. 2015, 6, 4966−4971

bands (blue lines in Figure 2b) below the CBM of the $[La_8Sr_2(SiO_4)_6]^{4+}$ framework (FCBM). These two bands are delocalized along the directions parallel to the *c*-axis (i.e., Γ−A and H−K) but localized along the directions perpendicular to the *c*-axis (i.e., A−H and K−Γ), implying a strong 1D anisotropy. In fact, the calculated effective masses of the light hole and electron (m_h* and m_e*, respectively) along the *c*-axis are $0.54m_0$ (along K−H) and $0.32m_0$ (along Γ−A), respectively, which are much smaller than those in $La_8Sr_2(SiO_4)_6O_2$ ($1.74m_0$ and $1.19m_0$, respectively). Contributions from any specific atoms in the $[La_8Sr_2(SiO_4)_6]^{4+}$ framework are excluded in forming the bonding and antibonding states of the four excess electrons. These states construct the lower and upper bands, respectively, and are largely confined in the channel formed by the 2*a* sites. Hence, they are referred to as interstitial states (the blue line in Figure 2c). Likewise, we call the two new bands channel bands (ChBs) hereafter. There is no nuclear bound to the interstitial states which are therefore loosely bound and dispersive. However, they strongly interact with the La 5*d* states (the wine line in Figure 2c), which mainly contribute to the CBM of the $[La_8Sr_2(SiO_4)_6]^{4+}$ framework (FCBM). It is worth noting that the energy levels of La 5*d* are much lower than those in $La_8Sr_2(SiO_4)_6O_2$ because of the reduced interatomic column repulsion upon extraction of two O(2*a*). As a result, $La_8Sr_2(SiO_4)_6$ exhibits a very narrow LDA band gap of ∼0.19 eV. Figure 2d shows the electron density on the $(1\bar{1}00)$ plane for the anionic states in the energy range from −1.0 to 0 eV. It can be clearly seen that these anionic states populate the 1D channel spaces along the *c*-axis and are perturbed only slightly by the coordinating La^{3+} cations, indicative of a 1D character of the anionic elections. Figure 2e illustrates the electron-localization function (ELF) of the total electron density on the $(1\bar{1}00)$ plane. Almost no electrons are observed between the channel and the $[La_8Sr_2(SiO_4)_6]^{4+}$ framework despite a weak presence of localized electrons in the space near the La^{3+} cations, substantiating the ionic bonding nature between the anionic states and the framework, which is similar to the Ca_2N and Y_2C cases.[26,29] These results indicate that $[La_8Sr_2(SiO_4)_6]^{4+}:4e^-$ is a semiconducting 1D electride.

For the experimental realization, single-phase $La_8Sr_2(SiO_4)_6O_2$ samples were synthesized at first through a solid-state reaction of precursor oxides. Its composition was confirmed by examining the powder samples using electron probe microanalyzer (EPMA) and was found to be $La_{7.94}Sr_{1.89}Si_{5.65}O_{26}$ by normalizing the oxygen stoichiometry, reasonably close the stoichiometric value. During the subsequent reducing reaction, the $La_8Sr_2(SiO_4)_6O_2$ pellets were sealed with titanium metal in an evacuated silica glass tube, followed by heating at 1200 °C for 72 h (refer to Supporting Information for detailed experimental procedures). The color of the $La_8Sr_2(SiO_4)_6O_2$ sample changed from white to gray upon this treatment (Figure S4 inset). X-ray diffraction (XRD) measurements revealed that the basic crystal structure of all the samples was maintained after the Ti treatment, and there were no extra peaks attributable to TiO_x which could be removed by polishing the pellet surface (Figure S4). Removal of the oxygen ions by the Ti metal from the sample bulk led to different unit cell parameters, as listed in Table S1. The decrease of the unit cell volume upon reduction is attributed mainly to the lattice shrinkage in the (*ab*) plane, rather than along the *c* axis, because the *c* parameter increases slightly. This observation is consistent with a prior study showing that incorporation of interstitial oxygen anions into the silicate apatite framework would lead to lattice expansion mainly on the same plane.[33]

Reduced apatite samples are investigated by electron paramagnetic resonance (EPR). The room temperature EPR spectrum displayed in Figure 3a shows a broad signal with a peak-to-peak width (ΔH_{pp}) of some 32 mT located at 344 mT (g_{app} = 2.051), suggesting the possible injection of electrons into the apatite lattice to form the F^+-like centers. Using $CuSO_4{\cdot}5H_2O$ as the reference, the spin concentration was determined to be ca. 7.7×10^{18} cm^{-3}. This quantity is similar to what was observed for the C12A7 electride (5×10^{19} cm^{-3}) derived from the calcium treatment.[17] However, it should be noted that the latter case exhibits a much sharper spectrum of 0.51 mT because of the fact that Ca has no nuclear moment. Hence, the noticeably large ΔH_{pp} value here might be a clue toward the existence of unresolved hyperfine splitting which is known to be a major factor contributing to the EPR line widths. In the current material the occurrence of hyperfine splitting is anticipated as long as the local magnetic field resulting from the nuclear moment of lanthanum (^{139}La: I = 7/2, NA = 99.911%; ^{138}La: I = 5, NA = 0.089%) is intense enough to affect the neighbor electrons. Therefore, the low-temperature EPR spectrum was subsequently collected at 77 K on the same sample as shown in Figure 3b where the hyperfine spectral lines become visible. To extract accurate parameters from the

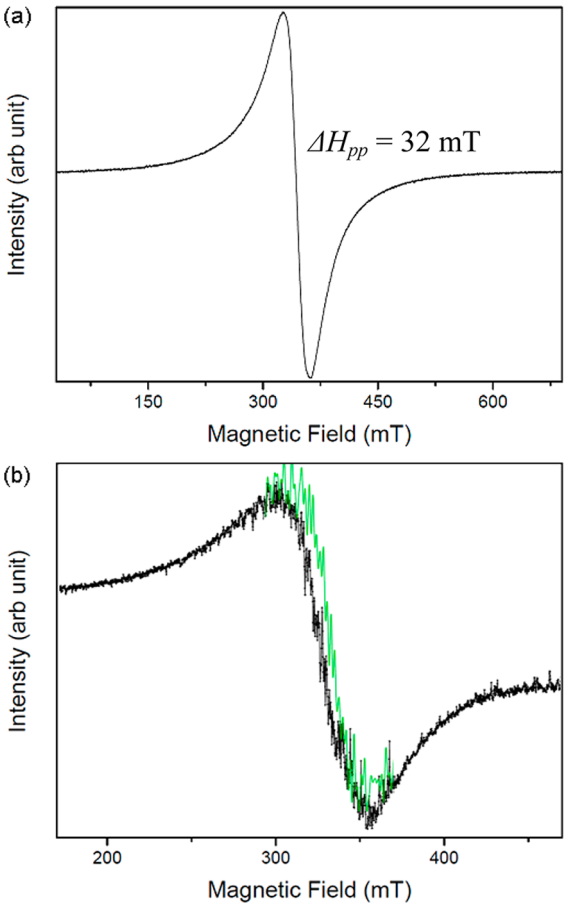

Figure 3. First-derivative X-band EPR spectra collected on the reduced $La_8Sr_2(SiO_4)_6O_2$ powder sample at (a) room temperature and (b) 77 K. The green line is a spectral simulation by considering the hyperfine interaction between the unpaired spin and neighboring La nuclei.

DOI: 10.1021/acs.jpclett.5b02283
J. Phys. Chem. Lett. 2015, 6, 4966−4971

experimental data, spectral simulations were performed using EasySpin.[37] The derived best fitting is found to be associated with a scenario that an unpaired electron couples to three equivalent La nuclei with the g tensors and hyperfine interaction constants of g_1 = 2.014, g_2 = 1.9579, and g_3 = 2.0501 and A_1 = 60, A_2 = 140, and A_3 = 176 MHz, respectively. Because these parameters indicate the local environment is close to an axial symmetry, the obtained results effectively mean that the compensating electrons occupy a position essentially close to the 2*a* oxygen site along the La channel, but not 2*b*. In other words, unpaired electrons are at the center of the La triangle (Figure 1). Complementarily, this position is in agreement with the calculated electron density map displayed in Figure 2d.

To quantify the amount of oxygen removed on reduction more accurately, small portions of powdered reduced apatite were heated in a thermogravimetric analyzer in oxygen. Weight change was small; however, weight gain of ∼0.17% was observed when the reduced sample was heated in pure dry O_2, as shown in Figure 4a. This weight change is equivalent to

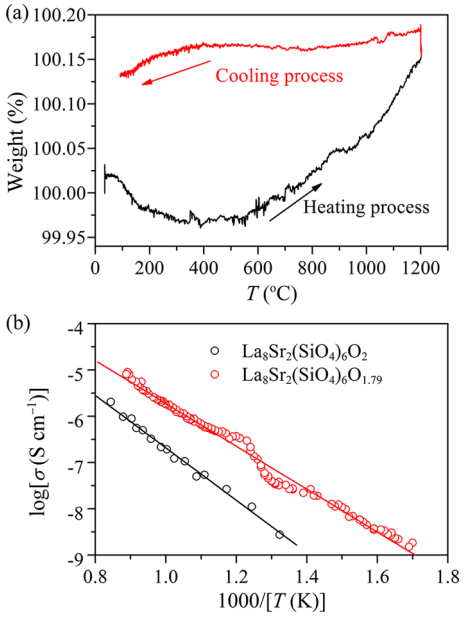

Figure 4. (a) Thermogravimetric analysis on the reduced $La_8Sr_2(SiO_4)_6O_2$ sample by heating at a rate of 5 °C/min in the dry O_2 atmosphere. (b) Electrical conductivities of $La_8Sr_2(SiO_4)_6O_2$ measured by AC impedance in air and reduced sample measured by DC conductivity measurement in 5% H_2/Ar.

replacing 0.21 of 2*a* oxygen in the $La_8Sr_2(SiO_4)_6O_2$ sample. In other words, the whole electron density in the reduced apatite sample is around 7.11 × 10^{20} cm^{-3}, a value three times smaller than that for $Ca_{12}Al_{14}O_{32}$:2e^-, 2.33 × 10^{21} cm^{-3}. The electrical conductivity of the same sample as displayed in Figure 4b was measured by the van der Pauw method in the temperature range of 300−1100 K using gold contacts. For comparison, the total oxide ion conductivity[33] for the original $La_8Sr_2(SiO_4)_6O_2$ pellet determined through AC impedance spectroscopy is also given in Figure 4b, although the charge carrier differs. The conducting performance of the parent phase is about 1 order of magnitude lower than the reduced sample. The conductivity variation with reciprocal temperature can be described by a typical Arrhenius-type behavior in the whole temperature range examined, which implies that the created electrons are not delocalized; thus, the conduction is controlled by a thermally activated hopping mechanism. The poor conducting behavior is associated with large activation energy (E_g) of ∼0.987 eV and related to the heavy effective mass of the electron, which will be discussed shortly. All these results point to the formation of a semiconducting electride $[La_8Sr_2(SiO_4)_6O_{1.79}]^{0.42+}$:0.42$e^-$.

To provide some insight into the electronic structure of the partially reduced apatite samples, we further performed DFT calculations for $La_8Sr_2(SiO_4)_6O_{2-x}$ (x = 0.5, 1.0, 1.5). The calculated band structures shown in Figure 5 exhibit decreasing

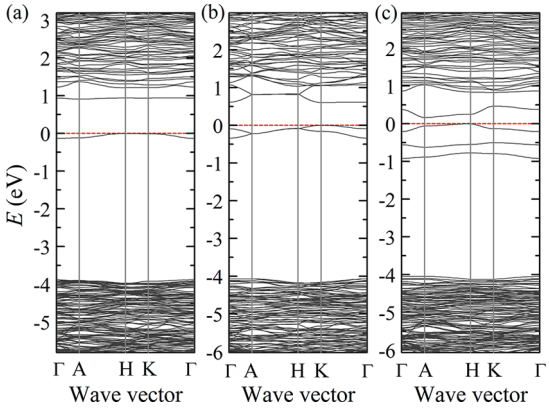

Figure 5. Band structures of $La_8Sr_2(SiO_4)_6O_{2-x}$ calculated with a 1 × 1 × 2 supercell: (a) x = 0.5, (b) x = 1, and (c) x = 1.5. The energies are aligned by O 2s orbitals for comparison.

band gaps from ∼0.9 to ∼0.2 eV as the x increases from 0.5 to 1.5. For x = 0.5, i.e., $La_8Sr_2(SiO_4)_6O_{1.5}$, the removal of 0.5 O(2*a*) results in localized interstitial valence and conduction bands, as shown in Figure 5a. The band dispersion along the directions parallel to the *c*-axis (i.e., Γ−A and H−K) are slightly narrower than that along the perpendicular directions (i.e., A−H and K−Γ), resulting in fairly heavy effective masses (m_h* = 34. 70m_0 and m_e* = 5.65m_0 along the *c*-axis). Accordingly, a poor carrier transport is expected for small x cases, e.g., x = 0.21 in Figure 4b. This is reasonable because for $x \le 0.5$, the average distance between two neighboring V_O (d_V) along the channel direction is ≥14.6 Å (i.e., 2*c*), much larger than the channel separation (d_{Ch}) of 9.6 Å, rendering the interaction between two neighboring V_O almost negligible. Therefore, different from $La_8Sr_2(SiO_4)_6$ (i.e., x = 2), $La_8Sr_2(SiO_4)_6O_{2-x}$ ($x \le 0.5$) do not exhibit a clear 1D-like characteristic. As x increase to 1.0 (i.e., half O(2*a*) atoms are removed), the d_V is ∼7.2 Å (i.e., *c*), slightly smaller than d_{Ch}. As a result, the interaction between two neighboring V_O significantly increases, leading to a wider band dispersion and thus a narrower band gap of 0.60 eV, as shown in Figure 5b. When x is further increased to 1.5 (i.e., $La_8Sr_2(SiO_4)_6O_{0.5}$), d_V decreases to ∼4.9 Å, much smaller than d_{Ch}. The band dispersion along the directions parallel to the *c*-axis (i.e., Γ−A and H−K) becomes wider while that along the perpendicular directions localized, which, to some degree, indicates a 1D-like anisotropy similar to the $[La_8Sr_2(SiO_4)_6]^{4+}$:4e^- case. More specifically, the resulting band gap of 0.17 eV, effective m_h* = 0.81m_0 and m_e* = 0.57m_0 along the *c*-axis are very close to those of $[La_8Sr_2(SiO_4)_6]^{4+}$:4e^-. From these results, to convert $La_8Sr_2(SiO_4)_6O_{2-x}$ into a real 1D electride, x should be larger than 1.5, that is, at least 75% of the O(2*a*) are removed.

The energy level of the channel oxygen in the rare earth silicate apatite is only 0.2−0.8 eV higher than those of the

DOI: 10.1021/acs.jpclett.5b02283
J. Phys. Chem. Lett. 2015, 6, 4966−4971

framework oxygens (Figure 2a), in contrast to the larger difference of ∼2 eV between the cage oxygens and the framework ones in C12A7.[22] Therefore, the present material is strongly stable against the reducing atmosphere and a deep O(2*a*) reduction requires hash conditions. However, what is most interesting is that the reduced derivative proves an air-stable property that is critically important for the new electride materials. In light of the current information, the channel spaces in the apatite structure allow 1D electride states. Hence, our results suggest a large family of candidate compounds for the synthesis of 1D electride materials whose enormous potential for practical utility is to be fully unleashed.

■ ASSOCIATED CONTENT

Supporting Information

The Supporting Information is available free of charge on the ACS Publications website at DOI: 10.1021/acs.jpclett.5b02283.

Detailed experimental procedures; three different partitions of La/Sr atoms in $La_8Sr_2(SiO_4)_6O_2$; and calculated band structures, structural parameters, densities, band gaps, and XRD patterns for all related apatite samples (PDF)

■ AUTHOR INFORMATION

Corresponding Author

*E-mail: hosono@msl.titech.ac.jp.

Present Address

[‖]Z.X.: Department of Physics & Astronomy and Wright Center for Photovoltaics Innovation and Commercialization, The University of Toledo, Toledo, OH 43606.

Author Contributions

[⊥]Y.Z. and Z.X. contributed equally to this work.

Notes

The authors declare no competing financial interest.

■ ACKNOWLEDGMENTS

Dr. S. Matsuishi is gratefully acknowledged for his assistance and technical support in collecting EPR spectra. This work was conducted under Tokodai Institute for Element Strategy (TIES) funded by MEXT through Elements Strategy Initiative to form Core Research Center, and the ACCEL Program by JST. The sponsorship to Y.Z. from MOE Key Laboratory of Physics and Technology for Advanced Batteries affiliated with Jilin University is acknowledged.

■ REFERENCES

(1) Markham, J. J. *F-Centers in Alkali Halides*; Academic Press: New York, 1966.

(2) Dye, J. L. Electrides: Ionic Salts with Electrons as the Anions. *Science* **1990**, *247*, 663−668.

(3) Dye, J. L. Electrons as Anions. *Science* **2003**, *301*, 607−608.

(4) Issa, D. B.; Dye, J. L. Synthesis of Cesium 18-Crown-6: The First Single-Crystal Electride. *J. Am. Chem. Soc.* **1982**, *104*, 3781−3782.

(5) Ellaboudy, A.; Dye, J. L.; Smith, P. B. Cesium 18-crown-6 compounds. A Crystalline Ceside and a Crystalline Electride. *J. Am. Chem. Soc.* **1983**, *105*, 6490−6491.

(6) Dawes, S. B.; Ward, D. L.; Huang, R. H.; Dye, J. L. First Electride Crystal Structure. *J. Am. Chem. Soc.* **1986**, *108*, 3534−3535.

(7) Huang, R. H.; Faber, M. K.; Moeggenborg, K. J.; Ward, D. L.; Dye, J. L. Structure of K+(cryptand[2.2.2]) Electride and Evidence for Trapped Electron Pairs. *Nature* **1988**, *331*, 599−601.

(8) Singh, D. J.; Krakauer, H.; Haas, C.; Pickett, W. W. Theoretical Determination That Electrons Act as Anions in the Electride Cs^+ (15-crown-5)$_2$·e^-. *Nature* **1993**, *365*, 39−42.

(9) Wagner, M. J.; Huang, R. H.; Eglin, J. L.; Dye, J. L. An Electride with a Large Six-Electron Ring. *Nature* **1994**, *368*, 726−729.

(10) Huang, R. H.; Wagner, M. J.; Gilbert, D. J.; ReidyCedergren, K. A.; Ward, D. L.; Faber, M. K.; Dye, J. L. Structure and Properties of Li^+(Cryptand [2.1.1])e^-, an Electride with a 1D "Spin-Ladder-like" Cavity-Channel Geometry. *J. Am. Chem. Soc.* **1997**, *119*, 3765−3772.

(11) Redko, M. Y.; Jackson, J. E.; Huang, R. H.; Dye, J. L. Design and Synthesis of a Thermally Stable Organic Electride. *J. Am. Chem. Soc.* **2005**, *127*, 12416−12422.

(12) Rencsok, R.; Kaplan, T. A.; Harrison, J. F. On the Electronic Structure of Electrides. *J. Chem. Phys.* **1990**, *93*, 5875−5882.

(13) Kaplan, T. A.; Rencsok, R.; Harrison, J. F. Valence-Electron Distribution of Cesium Crown-Ether Electrides. *Phys. Rev. B: Condens. Matter Mater. Phys.* **1994**, *50*, 8054.

(14) Dye, J. L. Electrides: Early Examples of Quantum Confinement. *Acc. Chem. Res.* **2009**, *42*, 1564−1572.

(15) Dye, J. L. Electrides: From 1D Heisenberg Chains to 2D Pseudo-Metals. *Inorg. Chem.* **1997**, *36*, 3816−3826.

(16) Hayashi, K.; Matsuishi, S.; Kamiya, T.; Hirano, M.; Hosono, H. Light-induced Conversion of an Insulating Refractory Oxide into a Persistent Electronic Conductor. *Nature* **2002**, *419*, 462−465.

(17) Matsuishi, S.; Toda, Y.; Miyakawa, M.; Hayashi, K.; Kamiya, T.; Hirano, M.; Tanaka, I.; Hosono, H. High-Density Electron Anions in a Nanoporous Single Crystal: $[Ca_{24}Al_{28}O_{64}]^{4+}(4e^-)$. *Science* **2003**, *301*, 626−629.

(18) Kim, S. W.; Shimoyama, T.; Hosono, H. Solvated Electrons in High-Temperature Melts and Glasses of the Room-Temperature Stable Electride $[Ca_{24}Al_{28}O_{64}]^{4+}$·$4e^-$. *Science* **2011**, *333*, 71−74.

(19) Lacerda, M.; Irvine, J. T. S.; Glasser, F. P.; West, A. R. High Oxide Ion Conductivity in $Ca_{12}Al_{14}O_{33}$. *Nature* **1988**, *332*, 525−526.

(20) Toda, Y.; Yanagi, H.; Ikenaga, E.; Kim, J. J.; Kobata, M.; Ueda, S.; Kamiya, T.; Hirano, M.; Kobayashi, K.; Hosono, H. Work Function of a Room-Temperature, Stable Electride $[Ca_{24}Al_{28}O_{64}]^{4+}(e^-)_4$. *Adv. Mater.* **2007**, *19*, 3564−3569.

(21) Irvine, J. T. S.; West, A. R. $Ca_{12}Al_{14}O_{33}$ — A Possible High-Temperature Moisture Sensor. *J. Appl. Electrochem.* **1989**, *19*, 410−412.

(22) Kim, S. W.; Matsuishi, S.; Nomura, T.; Kubota, Y.; Takata, M.; Hayashi, K.; Kamiya, T.; Hirano, M.; Hosono, H. Metallic State in a Lime-Alumina Compound with Nanoporous Structure. *Nano Lett.* **2007**, *7*, 1138−1143.

(23) Kitano, M.; Inoue, Y.; Yamazaki, Y.; Hayashi, F.; Kanbara, S.; Matsuishi, S.; Yokoyama, T.; Kim, S. W.; Hara, M.; Hosono, H. Ammonia Synthesis Using a Stable Electride as an Electron Donor and Reversible Hydrogen Store. *Nat. Chem.* **2012**, *4*, 934−940.

(24) Kitano, M.; Kanbara, S.; Inoue, Y.; Kuganathan, N.; Sushko, P. V.; Yokoyama, T.; Hara, M.; Hosono, H. Electride Support Boosts Nitrogen Dissociation over Ruthenium Catalyst and Shifts the Bottleneck in Ammonia Synthesis. *Nat. Commun.* **2015**, *6*, 6731.

(25) Toda, Y.; Hirayama, H.; Kuganathan, N.; Torrisi, A.; Sushko, P. V.; Hosono, H. Activation and Splitting of Carbon Dioxide on the Surface of an Inorganic Electride Material. *Nat. Commun.* **2013**, *4*, 2378.

(26) Lee, K.; Kim, S. W.; Toda, Y.; Matsuishi, S.; Hosono, H. Dicalcium Nitride as a Two-Dimensional Electride with an Anionic Electron Layer. *Nature* **2013**, *494*, 336−340.

(27) Steinbrenner, U.; Adler, P.; Hoelle, W.; Simon, A. Electronic Structure and Chemical Bonding in Alkaline Earth Metal Subnitrides: Photoemission Studies and Band Structure Calculations. *J. Phys. Chem. Solids* **1998**, *59*, 1527−1536.

(28) Inoshita, T.; Jeong, S.; Hamada, N.; Hosono, H. Exploration for Two-Dimensional Electrides via Database Screening and *Ab Initio* Calculation. *Phys. Rev. X* **2014**, *4*, 031023.

(29) Zhang, X.; Xiao, Z.; Lei, H.; Toda, Y.; Matsuishi, S.; Kamiya, T.; Ueda, S.; Hosono, H. Two-Dimensional Transition-Metal Electride Y_2C. *Chem. Mater.* **2014**, *26*, 6638−6643.

DOI: 10.1021/acs.jpclett.5b02283
J. Phys. Chem. Lett. 2015, 6, 4966−4971

(30) Tada, T.; Takemoto, S.; Matsuishi, S.; Hosono, H. High-Throughput *ab initio* Screening for Two-Dimensional Electride Materials. *Inorg. Chem.* **2014**, *53*, 10347−10358.
(31) White, T.; Ferraris, C.; Kim, J.; Madhavi, S. Apatite − An Adaptive Framework Structure. *Rev. Mineral. Geochem.* **2005**, *57*, 307−402.
(32) Slater, P. R.; Sansom, J. E. H.; Tolchard, J. R. Development of Apatite-Type Oxide Ion Conductors. *Chem. Rec.* **2004**, *4*, 373−384.
(33) Zhang, Y.; Su, Z.; Azad, A. K.; Zhou, W.; Irvine, J. T. S. Directly Imaging Interstitial Oxygen in Silicate Apatite. *Adv. Energy Mater.* **2012**, *2*, 316−321.
(34) Bechade, E.; Masson, O.; Iwata, T.; Julien, I.; Fukuda, K.; Thomas, P.; Champion, E. Diffusion Path and Conduction Mechanism of Oxide Ions in Apatite-Type Lanthanum Silicates. *Chem. Mater.* **2009**, *21*, 2508−2517.
(35) Kresse, G.; Furthmüller, J. Efficient Iterative Schemes for *ab initio* Total-Energy Calculations Using a Plane-Wave Basis Set. *Phys. Rev. B: Condens. Matter Mater. Phys.* **1996**, *54*, 11169.
(36) Ueda, K.; Hosono, H.; Hamada, N. Energy Band Structure of LaCuOCh (Ch = S, Se and Te) Calculated by the Full-Potential Linearized Augmented Plane-Wave Method. *J. Phys.: Condens. Matter* **2004**, *16*, 5179−5186.
(37) Stoll, S.; Schweiger, A. EasySpin, a Comprehensive Software Package for Spectral Simulation and Analysis in EPR. *J. Magn. Reson.* **2006**, *178*, 42−55.

DOI: 10.1021/acs.jpclett.5b02283
J. Phys. Chem. Lett. 2015, 6, 4966−4971